https://doi.org/10.1016/j.mechmat.2020.103496 This is the Pre-Published Version.

In-plane elasticity of regular hexagonal honeycombs with three different joints: A comparative study

Yu Chen, Hong Hu*

Institute of Textile and Clothing, The Hong Kong Polytechnic University, Hung Hom, Kowloon, Hong Kong, P. R. China

*The corresponding author:hu.hong@polyu.edu.hk (Hong Hu); Tel.: +852-3400-3089

Abstract: This paper is focused on the in-plane linear elastic properties of regular hexagonal honeycombs with three different joint geometries: hexagonal joint, circular joint and triangular joint. A combination of theoretical and finite element (FE) methods was adopted to investigate their in-plane elastic moduli (Young's modulus, shear modulus and Poisson's ratio), and a good agreement between the two methods was obtained. The influences of the geometric parameters on the elastic moduli, such as ρ^*/ρ_S and r/l, were fully discussed. Interestingly, a special relationship can exist among the three joint types, that is, the circular joint can be considered as a minimum circumscribed circle of the hexagonal and triangular joints. Based on this, a comparison among the honeycombs with three different types of joints was conducted. Compared to the conventional regular hexagonal honeycomb, the Young's modulus of the circular joint, hexagonal joint, and triangular joint honeycombs is enhanced by 61%, 80% and 431%, respectively; while the shear modulus is improved by 101%, 133% and 469%, respectively. Consequently, the triangular joint honeycomb was shown to be more successful in micro-structural layout compared with the other two types of honeycombs. This work could be a good guide for the design of novel cellular structures.

Keywords: Regular hexagonal honeycomb; Joint geometry; In-plane elasticity; Theoretical models; Finite element analysis

1. Introduction

The ideas from nature have inspired mankind to make a series of novel designs on high-performance materials and systems (Gibson and Ashby, 1997; Zhang et al., 2015). The conventional regular hexagonal honeycomb, which comes from the nest of the bees (Fig.1), has attracted considerable attention over the past few decades owing to its superior mechanical behaviors, such as high specific strength, specific stiffness and energy absorption. In practical applications, this kind of structure has often been used as core materials of sandwich panels. With the advancements in the use of sandwich panels, a better representation of the in-plane properties of the core materials was needed (Balawi and Abot, 2008). In this regard, a considerable number of efforts have been offered by the scientists. A beam model, that is fixed at one end

and guided at the other end, was firstly introduced by Abd El-Sayed et al. (1979) to predict the in-plane elastic moduli of the conventional regular hexagonal honeycomb. Similar to Abd El-Sayed et al. (Abd El-Sayed et al., 1979), Gibson and the co-authors (Gibson, 1981; Gibson et al., 1982; Gibson and Ashby, 1988) gave initial analytical expressions for the in-pane elastic moduli using the cell-wall bending model. Based on the cell-wall stretching and bending, Warren and Kraynik (1987) developed a new model to predict the in-plane elastic moduli. A refined cell wall's bending model by adding a beam's stretching and hinging motion was introduced by Masters and Evans (1996). Later on, improved models for the in-plane elastic moduli were proposed by Gibson and Ashby (1997) with fully considering shearing, stretching and bending of the cell walls. Recently, more accurate estimates of all nine elastic constants are obtained by modifying the analysis of Gibson and Ashby (1997) with consideration of the nodes at the intersection of the vertical and inclined members (Malek and Gibson, 2015; Sorohan et al., 2018). In addition, the finite element (FE) method and some advanced computational techniques were adopted to calculate the in-plane elastic moduli of this honeycomb (Shi and Tong, 1995; Gonella and Ruzzene, 2008; Reis and Ganghoffer, 2012; Catapano and Montemurro, 2014), and meanwhile, the experimental studies offered a better understanding of the in-plane elastic behavior (Balawi and Abot, 2008; Karakoi and Freund, 2012). Many scholars also paid attention to the in-plane large deformation of this honeycomb and its in-plane geometrical nonlinear behavior was studied based on the elastic bending theory of beam in large deflection (Lan and Fu, 2009; Zhu and Mills, 2000; Qiu et al., 2016). Furthermore, the in-pane quasi static and dynamic crushing behaviors were well documented (Papka and Kyriakides, 1994; Ruan et al., 2003; Hu and Yu, 2010; Cricrì et al., 2013; Zhang et al., 2018).

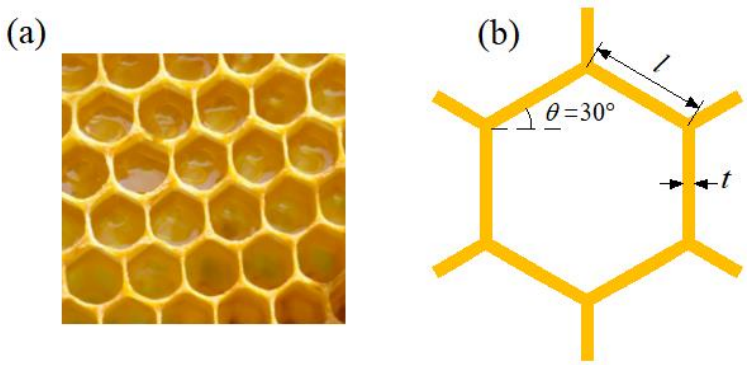

Fig.1. (a) Natural honeycomb; (b) regular hexagonal honeycomb. (Color online only)

It is known that the macro mechanical properties of cellular structures depend on their microstructures. This stimulates people to think about how to improve the existing cellular structures by tailoring their micro layouts. Under this consideration, a large number of successful attempts have been made based on the conventional regular hexagonal honeycomb. For instance, a regular hexagonal honeycomb is modified into a re-entrant form to achieve a negative Poisson's ratio (Gibson and Ashby, 1997). A hierarchical design strategy that replaces the solid cell walls of the conventional regular hexagonal honeycomb with specific substructures can greatly

increase the in-plane stiffness (Sun et al., 2015). It was found by Zorzetto and Ruffoni (2017) that a re-entrant inclusion acting as a defect into the regular hexagonal honeycomb is sufficient to generate a substantial augmentation in stiffness. In addition, a lot of attention has also been paid to the influence of three-wall joint geometry in the conventional regular hexagonal honeycomb. The geometry of three cell walls connected at a vertex with Plateau borders was analyzed and employed to represent a repeating element for regular hexagonal honeycomb (Chuang and Huang, 2002a). The effects of the Plateau borders on the macro elastic moduli, buckling and plastic collapse strength were analyzed (Chuang and Huang, 2002a; Chuang and Huang, 2002b). In recent years, a new type of hierarchical honeycomb was proposed by replacing every three-wall vertex of a regular hexagonal lattice with a smaller hexagon, as illustrated in Fig.2(a) (Ajdari et al., 2012). Chen et al. (2014) constructed a new honeycomb by replacing the three-wall joint of the regular hexagonal honeycomb with a hollow-cylindrical joint (i.e., circular joint, see Fig.2(b)), and developed a corresponding theory to study its mechanical properties, including Young's modulus, Poisson's ratio, fracture strength and stress intensity factor. Another homologous honeycomb was conceived by Pozniak et al. (2013) via replacing every three-wall vertex of a regular hexagonal lattice with a small triangle (Fig.2(c)).

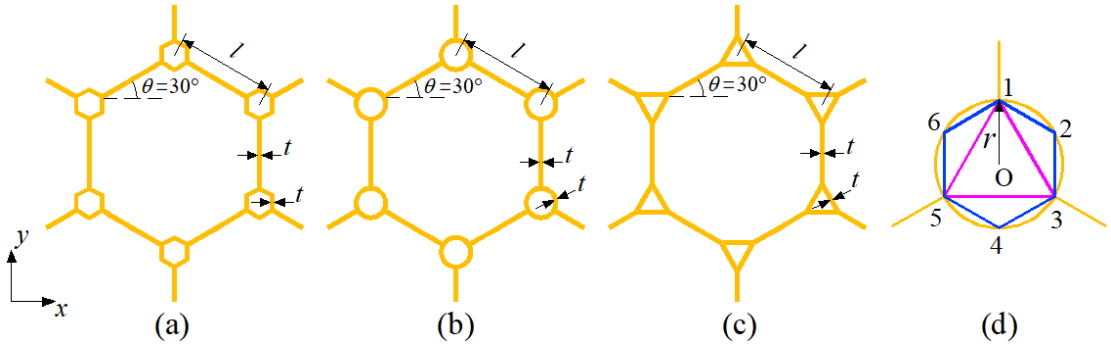

Fig.2. (a) Hexagonal joint honeycomb; (b) circular joint honeycomb; (c) triangular joint honeycomb; (d) a schematic comparison of the three joint types. (Color online only)

The configurations listed in Fig.2 (a), (b) and (c) form the basis of this paper. Although discussion on the mechanical properties of these honeycombs has been reported in the literature, some additions are still needed. Until now, only the in-plane large deformation of the triangular joint honeycomb has been investigated by Pozniak et al. using the FE method (Pozniak et al., 2013). Theoretical models for the in-plane elastic moduli of the triangular joint honeycomb under small deformation are not found in the available literature. Ajdari and the co-workers (Ajdari et al., 2012) have given an analytical model to successfully predict the in-plane Young's modulus and Poisson's ratio of the hexagonal joint honeycomb. However, only bending deformation of cell walls was considered in this model as axial and shear deformations were ignored. This may make this model unsuitable for moderately stubby beam structures. Also, it is very interesting to note that, a special relationship can exist among the three mentioned joint types, as shown in Fig.2(d). The circular

joint can be considered as a minimum circumscribed circle of the hexagonal and triangular joints. Naturally, a curious issue arises: which configuration is optimal in mechanical properties. Given above, the work in this paper is organized as follows. Firstly, we developed a theoretical model to predict the in-plane elastic moduli (i.e., Young's modulus, Poisson's ratio and shear modulus) of the three honeycombs with fully considering the axial and shear deformations of each cell wall in addition to the bending deformation. Secondly, FE analysis on the three types of honeycombs under small deformation was carried out by using ANSYS, and compared with the theoretical results. The effects of micro geometric parameters on the macro elastic moduli of these honeycombs were further discussed. Finally, a comparison among these honeycombs was also presented.

2. Geometries of the honeycombs

The honeycombs with three different joint geometries in this study are based on the conventional regular hexagonal honeycomb whose basic geometric parameters, including slant angle ($\theta = 30°$), cell wall thickness (t), and cell wall length (l), are illustrated in Fig.1. The basic geometric details of these honeycombs are consistent with those of the conventional regular hexagonal honeycomb, as shown in Fig.2 (a), (b) and (c). The radius for the circular joint is r. As mentioned before, the circular joint in this paper can be considered as a minimum circumscribed circle of the hexagonal and triangular joints. Hence, the length of the walls within the hexagonal joint in Fig.2(d) is:

$$l_{12} = l_{23} = l_{34} = l_{45} = l_{56} = l_{61} = r\,. \tag{1}$$

Similarly, the length of the walls within the triangular joint (Fig.2(d)) is:

$$l_{13} = l_{35} = l_{51} = \sqrt{3}r\,. \tag{2}$$

The relative density for the conventional regular hexagonal honeycomb can be approximately expressed as:

$$\frac{\rho_{cr}^{*}}{\rho_s} = \frac{2}{\sqrt{3}}\frac{t}{l}, \tag{3}$$

while that for the circular joint, hexagonal joint and triangular joint honeycomb is:

$$\frac{\rho_{c}^{*}}{\rho_s} = \frac{4}{\sqrt{3}}\frac{t}{l}\left[\frac{1}{2} + \left(\frac{2\pi}{3} - 1\right)\frac{r}{l}\right], \tag{4}$$

$$\frac{\rho_{h}^{*}}{\rho_s} = \frac{4}{\sqrt{3}}\frac{t}{l}\left(\frac{1}{2} + \frac{r}{l}\right), \tag{5}$$

and

$$\frac{\rho_{t}^{*}}{\rho_s} = \frac{4}{\sqrt{3}}\frac{t}{l}\left[\frac{1}{2} + \left(\sqrt{3} - 1\right)\frac{r}{l}\right], \tag{6}$$

respectively，where ρ^* and ρ_s denote the density of the honeycombs and the basic material, respectively.

3. Equivalent elastic moduli

3.1. Young's moduli and Poisson's ratios

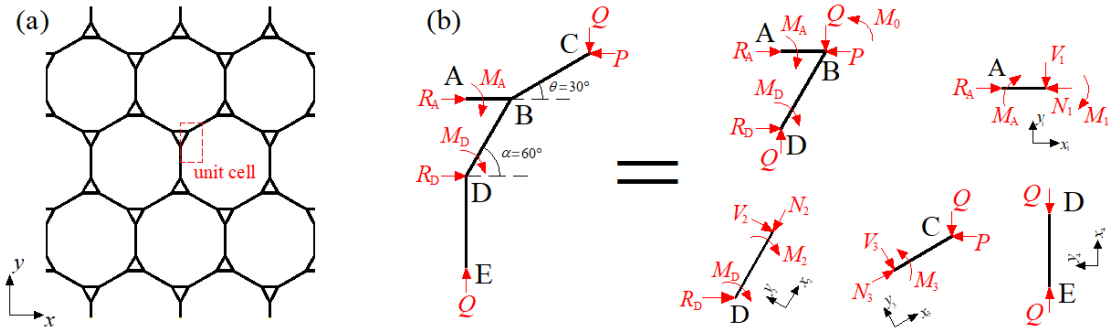

Fig.3. (a) Unit cell for the triangular joint honeycomb and (b) force analysis in a unit cell: unit cell under a *x*- directional uniaxial load P or a *y*- directional uniaxial load Q. x_i-y_i denotes the local coordinate system for each wall. (Color online only)

In this section, the Young's modulus and Poisson's ratio of the triangular joint honeycomb will be theoretically investigated by using Castigliano's method. According to the structural symmetry, a unit cell as outlined in Fig.3(a) was determined for analysis. In the unit cell, there is no moment acting at points C and E as they are the midpoint (symmetry point). The thickness of the cell walls AB, BC and BD is t while that of the wall DE is $\frac{t}{2}$. The lengths of the walls AB, BC, BD and DE are $\frac{\sqrt{3}}{2}r$, $\frac{l}{2}-r$, $\sqrt{3}r$ and $\frac{l}{2}-r$, respectively. The slant angles of the walls BC and BD are $\theta=30°$ and $\alpha=60°$, respectively.

The analytical model for the structure under *x*- or *y*- directional loading is shown in Fig.3(b), in which R_A and R_D are the reaction horizontal forces while M_A and M_D are the reaction moments when the honeycomb undergoes a uniaxial load P or Q. It should be pointed out that, for *x*- directional loading, the force P is an actual load but the force Q is not an actual load, it is rather a dummy force so Castigliano's method can be used for *y*- directional strain. Similarly, the *x*- directional force P is an imaginary load when loading along the *y*- direction.

From Fig.3(b), the total strain energy stored in the unit cell ABCDE, U_1, is

composed of four components, i.e.,

$$U_1 = U_{AB} + U_{BC} + U_{BD} + U_{DE}, \tag{7}$$

where U_{AB}, U_{BC}, U_{BD} and U_{DE} are the strain energies stored in the cell walls AB, BC, BD and DE, respectively. We can obtain the strain energy stored in each wall on the basic of force analysis, as shown in Fig.3(b). For each wall, N_i, V_i and M_i denote the axial force, shear force and bending moment acting on it. The axial force, shear force and bending moment for the walls are listed below:

AB: $N_1(x_1) = R_A$, $V_1(x_1) = 0$, $M_1(x_1) = -M_A$;

BD: $N_2(x_2) = R_D \cos\alpha + Q\sin\alpha$, $V_2(x_2) = Q\cos\alpha - R_D \sin\alpha$,

$M_2(x_2) = -M_D - (Q\cos\alpha - R_D \sin\alpha)x_2$;

BC: $N_3(x_3) = P\cos\theta + Q\sin\theta$, $V_3(x_3) = P\sin\theta - Q\cos\theta$,

$M_3(x_3) = -(P\sin\theta - Q\cos\theta)(l/2 - r - x_3)$;

DE: $N_4(x_4) = Q$, $V_4(x_4) = 0$, $M_4(x_4) = 0$.

By simultaneously considering three types of strain energies associated to bending, tensile and shear loading, the strain energy for each wall can be calculated by using a unified formula:

$$U = \int_0^x \frac{N^2(x)}{2E_s A}dx + \int_0^x \frac{kV^2(x)}{2G_s A}dx + \int_0^x \frac{M^2(x)}{2E_s I}dx, \tag{8}$$

where U is the strain energy stored in the wall, $N(x)$, $V(x)$ and $M(x)$ respectively denote the axial force, shear force and bending moment for the wall. E_s and G_s are the instinct Young's modulus and shear modulus of the basic material, respectively, and for isotropic material $G_s = E_s/[2(1+\nu_s)]$ (ν_s is the instinct Poisson's ratio of the basic material). $k = 6/5$ is the shear coefficient for a rectangular cross section. $I = bt^3/12$ is the second moment of area and $A = bt$ is the area of the cross section; b denotes the out-of-plane depth of the honeycomb.

Therefore, the strain energy stored in each wall is:

$$U_{\mathrm{AB}}=\frac{\sqrt{3}R_{\mathrm{A}}{}^{2}r}{4E_sA}+\frac{\sqrt{3}M_{\mathrm{A}}{}^{2}r}{4E_sI};$$

$$U_{\mathrm{BD}}=\frac{\sqrt{3}\left(R_{\mathrm{D}}\cos\alpha+Q\sin\alpha\right)^2 r}{2E_sA}+\frac{\sqrt{3}k\left(Q\cos\alpha-R_{\mathrm{D}}\sin\alpha\right)^2 r}{2G_sA}+\frac{\sqrt{3}M_{\mathrm{D}}{}^{2}r}{2E_sI}+\frac{\sqrt{3}\left(Q\cos\alpha-R_{\mathrm{D}}\sin\alpha\right)^2 r^3}{2E_sI}$$
$$-\frac{3M_{\mathrm{D}}\left(Q\cos\alpha-R_{\mathrm{D}}\sin\alpha\right)r^2}{2E_sI};$$

$$U_{\mathrm{BC}}=\frac{\left(P\cos\theta+Q\sin\theta\right)^2\left(l/2-r\right)}{2E_sA}+\frac{k\left(P\sin\theta-Q\cos\theta\right)^2\left(l/2-r\right)}{2G_sA}+\frac{\left(P\sin\theta-Q\cos\theta\right)^2\left(l/2-r\right)^3}{6E_sI};$$

$$U_{\mathrm{DE}}=\frac{Q^2\left(l/2-r\right)}{E_sA}.$$

(9)

where $M_0=\left(P\sin\theta-Q\cos\theta\right)\left(l/2-r\right)$. Due to the force balance conditions in ABD as shown in Fig.3(b), we have $M_{\mathrm{D}}=M_0+3R_{\mathrm{D}}r/2-M_{\mathrm{A}}-\sqrt{3}Qr/2$ and $R_{\mathrm{D}}=P-R_{\mathrm{A}}$. Considering the zero x- directional displacement and zero rotation of point A due to the structural symmetry, one can write $\partial U_1/\partial R_{\mathrm{A}}=0$ and $\partial U_1/\partial M_{\mathrm{A}}=0$. Then we have,

$$\begin{cases}\left[\frac{\sqrt{3}r\left(1+2\cos^2\alpha\right)}{2E_sA}+\frac{r^3\left(9\sqrt{3}-18\sin\alpha+4\sqrt{3}\sin^2\alpha\right)}{4E_sI}+\frac{\sqrt{3}kr\sin^2\alpha}{G_sA}\right]\cdot R_{\mathrm{A}}+\frac{3r^2\left(\sqrt{3}-\sin\alpha\right)}{2E_sI}\cdot M_{\mathrm{A}}=\\ \frac{\sqrt{3}r\cos\alpha\left(P\cos\alpha+Q\sin\alpha\right)}{E_sA}+\frac{\sqrt{3}kr\sin\alpha\left(P\sin\alpha-Q\cos\alpha\right)}{G_sA}+\\ \frac{6M_0r^2\left(\sqrt{3}-\sin\alpha\right)+Qr^3\left(9\cos\alpha-9+3\sqrt{3}\sin\alpha-2\sqrt{3}\sin 2\alpha\right)+Pr\left(9\sqrt{3}-18\sin\alpha+4\sqrt{3}\sin^2\alpha\right)}{4E_sI};\\ \frac{3r^2\left(\sqrt{3}-\sin\alpha\right)}{2E_sI}\cdot R_{\mathrm{A}}+\frac{3\sqrt{3}r}{2E_sI}\cdot M_{\mathrm{A}}=\frac{2\sqrt{3}M_0r+3Qr^2\left(\cos\alpha-1\right)+3Pr^2\left(\sqrt{3}-\sin\alpha\right)}{2E_sI}.\end{cases}$$

(10)

From the two relations in Eq.(10), R_{A} and M_{A} can be calculated as a known function of P and Q. By substituting the calculated R_{A} and M_{A} into Eqs.(9) and (7), the total strain energy stored in the unit cell ABCED, U_1, can thereby be expressed as a known function of P and Q. When the honeycomb undergoes a x-directional uniaxial load, i.e. $Q=0$, then the x- and y- directional displacements of

point C due to force P can be calculated as follows, respectively: $\delta_x^{\mathrm{C}} = \left(\partial U_1/\partial P\right)\big|_{Q=0}$; $\delta_y^{\mathrm{C}} = \left(\partial U_1/\partial Q\right)\big|_{Q=0}$. Hence, the equivalent strains along the x- and y- directions are $\varepsilon_x = 2\delta_x^{\mathrm{C}}/\left(l\cos\theta\right)$ and $\varepsilon_y = 2\delta_y^{\mathrm{C}}/\left(l+l\sin\theta\right)$, respectively. The x- directional equivalent stress σ_x can be expressed as: $\sigma_x = P/\left[\left(l+l\sin\theta\right)b\right]$. Finally, the Young's modus (E_x) and Poisson's ratio (ν_{xy}) can be calculated by $E_x = \sigma_x/\varepsilon_x$ and $\nu_{xy} = -\varepsilon_y/\varepsilon_x$, respectively.

Similarly, in the case of y- directional loading, i.e., $P=0$. the x- and y- directional displacements of point C due to the force Q can be respectively calculated as: $\delta_x^{\mathrm{C}} = \left(\partial U_1/\partial P\right)\big|_{P=0}$; $\delta_y^{\mathrm{C}} = \left(\partial U_1/\partial Q\right)\big|_{P=0}$. The equivalent stress along the y direction is $\sigma_y = Q/\left(l\cos\theta b\right)$ and thus the corresponding Young's modulus (E_y) and Poisson's ratio (ν_{yx}) can be obtained.

Concerning the hexagonal joint honeycomb, full deformation mechanisms of each cell wall will be accurately considered. The free body diagram of the unit cell of the hexagonal joint honeycomb is displayed in Fig.A.1, and the details are shown in Appendix A. For completeness, similar derivations for the Young's modulus and Poisson's ratio of the circular joint honeycomb are also presented in this paper, although Chen et al. (2014) have given a theoretical model. Its unit cell and the corresponding free body diagram are illustrated in Fig.B.1. The details are shown in Appendix B. It should be noted that, the current derivation for the Poisson's ratio of the circular joint honeycomb is more straightforward than that developed by Chen et al. (Chen et al., 2014).

It has been shown that periodic boundary conditions are ideally suited for predicting the mechanical properties of a periodic media (Xia et al., 2003; Ai and Gao, 2018). In order to provide reference solutions and evaluate the theoretical models developed in this paper, we simulated the in-plane linear elastic responses of these honeycombs by using the FE method with periodic boundary conditions. The periodic boundary conditions for a cubic media subjected to a prescribed strain ε_{ij}^0 are given by (Ai and Gao, 2018):

$$\left.\begin{aligned} u_i^{k^+} - u_i^{k^-} &= \varepsilon_{ij}^0\left(x_j^{k^+} - x_j^{k^-}\right), \\ \varphi_i^{k^+} &= \varphi_i^{k^-}. \end{aligned}\right\},\ i,j \in \{x,y,z\}. \tag{11}$$

where $x_j^{k^+}$ and $x_j^{k^-}$ respectively denote the coordinates of the matched nodes k^+

and k^- on the cubic media boundary along the $j-$ direction. $u_i^{k^+}$ and $x_i^{k^-}$ respectively denote the displacement components of the nodes k^+ and k^- while $\varphi_i^{k^+}$ and $\varphi_i^{k^-}$ are, respectively, the rotation components of the nodes k^+ and k^-.

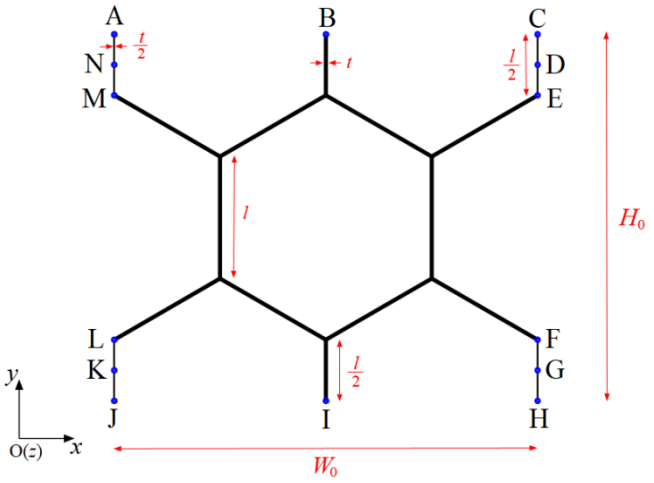

Fig.4. Representative block for the conventional regular hexagonal honeycomb. Points A to N denote the nodes at the boundaries of the discretized representative block. (Color online only)

Firstly, we would take the conventional regular hexagonal honeycomb as an example to calculate its in-plane elastic moduli by using the FE method with periodic boundary conditions. Then, the obtained elastic moduli would be further compared with the experimental and analytical results obtained by Gibson and Ashby (1997) in order to verify the rationality of the FE models we used. The representative block for the conventional regular hexagonal honeycomb, as illustrated in Fig.4, was modeled by using ANSYS 16.0. Conventional regular hexagonal honeycombs with seven different levels of t/l were investigated. These t/l values were obtained by fixing $l=20\text{mm}$ while varying t as 2.655mm, 2.932mm, 3.198mm, 3.463mm, 3.718mm, 3.972mm and 4.214mm. The macro dimension of the representative block is 69.282mm (W_0) × 60mm (H_0) ×1mm (b), as shown in Fig.4 (b is the out-of-plane depth). All models were meshed using Beam 188 which is based on Timoshenko beam theory, and thus it is suitable for analyzing slender to moderately stubby beam structures. Aluminum alloy with its Young's modulus $E_s=70\text{GPa}$ and Poisson's ratio $\nu_s=0.3$ was used for the cell wall material. A free meshing scheme with the 1mm mesh size was implemented to the FE models. According to Eq. (11), the periodic boundary conditions were applied by using the 'Constraint Equation' function in ANSYS. In the case of the discretized representative block in Fig.4, detailed boundary conditions for three different loading cases are listed as follows:

(a) Periodic boundary conditions for uniaxial loading in the x- direction:

$$
\begin{aligned}
&u_y^{\mathrm{C}}=u_y^{\mathrm{A}},\ u_y^{\mathrm{D}}=u_y^{\mathrm{N}},\ u_y^{\mathrm{E}}=u_y^{\mathrm{M}},\ u_y^{\mathrm{F}}=u_y^{\mathrm{L}},\ u_y^{\mathrm{G}}=u_y^{\mathrm{K}},\ u_y^{\mathrm{H}}=u_y^{\mathrm{J}},\\
&\varphi_z^{\mathrm{C}}=\varphi_z^{\mathrm{A}},\ \varphi_z^{\mathrm{D}}=\varphi_z^{\mathrm{N}},\ \varphi_z^{\mathrm{E}}=\varphi_z^{\mathrm{M}},\ \varphi_z^{\mathrm{F}}=\varphi_z^{\mathrm{L}},\ \varphi_z^{\mathrm{G}}=\varphi_z^{\mathrm{K}},\ \varphi_z^{\mathrm{H}}=\varphi_z^{\mathrm{J}},\\
&\varphi_z^{\mathrm{A}}=\varphi_z^{\mathrm{J}},\ \varphi_z^{\mathrm{B}}=\varphi_z^{\mathrm{I}},\ \varphi_z^{\mathrm{C}}=\varphi_z^{\mathrm{H}},\\
&u_x^{\mathrm{C}}-u_x^{\mathrm{A}}=\varepsilon_{xx}^0W_0,\ u_x^{\mathrm{D}}-u_x^{\mathrm{N}}=\varepsilon_{xx}^0W_0,\ u_x^{\mathrm{E}}-u_x^{\mathrm{M}}=\varepsilon_{xx}^0W_0,\\
&u_x^{\mathrm{F}}-u_x^{\mathrm{L}}=\varepsilon_{xx}^0W_0,\ u_x^{\mathrm{G}}-u_x^{\mathrm{K}}=\varepsilon_{xx}^0W_0,\ u_x^{\mathrm{H}}-u_x^{\mathrm{J}}=\varepsilon_{xx}^0W_0,\\
&u_y^{\mathrm{A}}-u_y^{\mathrm{J}}=u_y^{\mathrm{B}}-u_y^{\mathrm{I}}=u_y^{\mathrm{C}}-u_y^{\mathrm{H}},\\
&u_z^{\mathrm{J}}=u_y^{\mathrm{J}}=u_x^{\mathrm{J}}=\varphi_z^{\mathrm{J}}=\varphi_y^{\mathrm{J}}=\varphi_x^{\mathrm{J}}=0\ \text{(to eliminate the rigid body motion)}
\end{aligned}
\tag{12}
$$

(b) Periodic boundary conditions for uniaxial loading in the y- direction:

$$
\begin{aligned}
&u_y^{\mathrm{C}}=u_y^{\mathrm{A}},\ u_y^{\mathrm{D}}=u_y^{\mathrm{N}},\ u_y^{\mathrm{E}}=u_y^{\mathrm{M}},\ u_y^{\mathrm{F}}=u_y^{\mathrm{L}},\ u_y^{\mathrm{G}}=u_y^{\mathrm{K}},\ u_y^{\mathrm{H}}=u_y^{\mathrm{J}},\\
&\varphi_z^{\mathrm{C}}=\varphi_z^{\mathrm{A}},\ \varphi_z^{\mathrm{D}}=\varphi_z^{\mathrm{N}},\ \varphi_z^{\mathrm{E}}=\varphi_z^{\mathrm{M}},\ \varphi_z^{\mathrm{F}}=\varphi_z^{\mathrm{L}},\ \varphi_z^{\mathrm{G}}=\varphi_z^{\mathrm{K}},\ \varphi_z^{\mathrm{H}}=\varphi_z^{\mathrm{J}},\\
&\varphi_z^{\mathrm{A}}=\varphi_z^{\mathrm{J}},\ \varphi_z^{\mathrm{B}}=\varphi_z^{\mathrm{I}},\ \varphi_z^{\mathrm{C}}=\varphi_z^{\mathrm{H}},\\
&u_y^{\mathrm{A}}-u_y^{\mathrm{J}}=\varepsilon_{yy}^0H_0,\ u_y^{\mathrm{B}}-u_y^{\mathrm{I}}=\varepsilon_{yy}^0H_0,\ u_y^{\mathrm{C}}-u_y^{\mathrm{H}}=\varepsilon_{yy}^0H_0,\\
&u_x^{\mathrm{C}}-u_x^{\mathrm{A}}=u_x^{\mathrm{D}}-u_x^{\mathrm{N}}=u_x^{\mathrm{E}}-u_x^{\mathrm{M}}=u_x^{\mathrm{F}}-u_x^{\mathrm{L}}=u_x^{\mathrm{G}}-u_x^{\mathrm{K}}=u_x^{\mathrm{H}}-u_x^{\mathrm{J}},\\
&u_z^{\mathrm{J}}=u_y^{\mathrm{J}}=u_x^{\mathrm{J}}=\varphi_z^{\mathrm{J}}=\varphi_y^{\mathrm{J}}=\varphi_x^{\mathrm{J}}=0\ \text{(to eliminate the rigid body motion)}
\end{aligned}
\tag{13}
$$

(c) Periodic boundary conditions for the in-plane shear loading:

$$
\begin{aligned}
&u_x^{\mathrm{C}}=u_x^{\mathrm{A}},\ u_x^{\mathrm{D}}=u_x^{\mathrm{N}},\ u_x^{\mathrm{E}}=u_x^{\mathrm{M}},\ u_x^{\mathrm{F}}=u_x^{\mathrm{L}},\ u_x^{\mathrm{G}}=u_x^{\mathrm{K}},\ u_x^{\mathrm{H}}=u_x^{\mathrm{J}},\\
&u_y^{\mathrm{A}}=u_y^{\mathrm{J}},\ u_y^{\mathrm{B}}=u_y^{\mathrm{I}},\ u_y^{\mathrm{C}}=u_y^{\mathrm{H}},\ \varphi_z^{\mathrm{A}}=\varphi_z^{\mathrm{J}},\ \varphi_z^{\mathrm{B}}=\varphi_z^{\mathrm{I}},\ \varphi_z^{\mathrm{C}}=\varphi_z^{\mathrm{H}},\\
&\varphi_z^{\mathrm{C}}=\varphi_z^{\mathrm{A}},\ \varphi_z^{\mathrm{D}}=\varphi_z^{\mathrm{N}},\ \varphi_z^{\mathrm{E}}=\varphi_z^{\mathrm{M}},\ \varphi_z^{\mathrm{F}}=\varphi_z^{\mathrm{L}},\ \varphi_z^{\mathrm{G}}=\varphi_z^{\mathrm{K}},\ \varphi_z^{\mathrm{H}}=\varphi_z^{\mathrm{J}},\\
&u_y^{\mathrm{C}}-u_y^{\mathrm{A}}=\varepsilon_{xy}^0W_0,\ u_y^{\mathrm{D}}-u_y^{\mathrm{N}}=\varepsilon_{xy}^0W_0,\ u_y^{\mathrm{E}}-u_y^{\mathrm{M}}=\varepsilon_{xy}^0W_0,\\
&u_y^{\mathrm{F}}-u_y^{\mathrm{L}}=\varepsilon_{xy}^0W_0,\ u_y^{\mathrm{G}}-u_y^{\mathrm{K}}=\varepsilon_{xy}^0W_0,\ u_y^{\mathrm{H}}-u_y^{\mathrm{J}}=\varepsilon_{xy}^0W_0,\\
&u_x^{\mathrm{A}}-u_x^{\mathrm{J}}=\varepsilon_{xy}^0H_0,\ u_x^{\mathrm{B}}-u_x^{\mathrm{I}}=\varepsilon_{xy}^0H_0,\ u_x^{\mathrm{C}}-u_x^{\mathrm{H}}=\varepsilon_{xy}^0H_0,\\
&u_z^{\mathrm{J}}=u_y^{\mathrm{J}}=u_x^{\mathrm{J}}=\varphi_z^{\mathrm{J}}=\varphi_y^{\mathrm{J}}=\varphi_x^{\mathrm{J}}=0\ \text{(to eliminate the rigid body motion)}
\end{aligned}
\tag{14}
$$

In this study, the prescribed strain ε_{ij}^0 were considered equal for all load cases, i.e., $\varepsilon_{xx}^0=\varepsilon_{yy}^0=\varepsilon_{xy}^0=0.01$. In the case of x- directional uniaxial loading, the x-directional resultant force F_x can be obtained by using 'Nodal Loads' function in ANSYS with exporting the x- directional total forces of the nodes at the right boundary, i.e., nodes C, D, E, F, G and H in Fig.4. Similarly, the y- directional resultant force F_y can be obtained by exporting the y- directional total forces of the nodes A, B and C in Fig.4 for y- directional uniaxial loading case, while the shear force (T_x) along the x- direction can be obtained by exporting the x- directional total

forces of the nodes A, B and C. Therefore, the equivalent averaged stresses are defined as:

$$\sigma_{xx} = \frac{F_x}{H_0 b},\ \sigma_{yy} = \frac{F_y}{W_0 b},\ \sigma_{xy} = \frac{T_x}{W_0 b} \tag{15}$$

Then the equivalent elastic Young's modulus and shear modulus are given as:

$$E_x = \frac{\sigma_{xx}}{\varepsilon^0_{xx}},\ E_y = \frac{\sigma_{yy}}{\varepsilon^0_{yy}},\ G_{xy} = \frac{\sigma_{xy}}{2\varepsilon^0_{xy}} \tag{16}$$

We have found in the FE results that nodes A, B and C have an equal y- directional displacement, Δu_y, for x- directional uniaxial loading, while nodes C, D, E, F, G and H have an equal x- directional displacement, Δu_x, for y- directional uniaxial loading. Consequently, the equivalent Poisson's ratio for the honeycombs can be given as,

$$\nu_{xy} = -\frac{\Delta u_y}{H_0 \varepsilon^0_{xx}},\ \nu_{yx} = -\frac{\Delta u_x}{W_0 \varepsilon^0_{yy}} \tag{17}$$

Fig.5 displays a comparison between the current calculated elastic moduli and those obtained in the available literature (Gibson, 1981; Gibson and Ashby, 1997). Obviously, the current FE results are quite close to both the experiments and analytical results, which helps to verify the FE models we used.

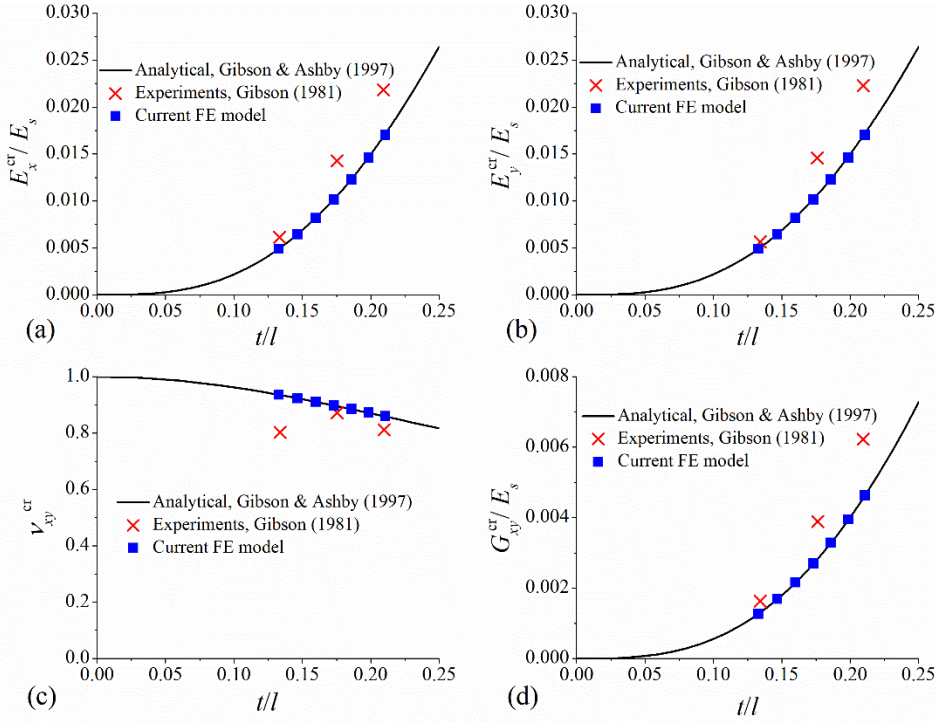

Fig.5. In-plane elastic moduli of the conventional hexagonal honeycomb: Comparisons between analytical model predictions of Gibson and Ashby (1997), experimental data (Gibson, 1981) and current FE predictions. (Color online only)

Next, the similar FE analyzing procedure would be adopted to study the hexagonal honeycombs with three different joint geometries. Here, honeycombs with five r/l values (r/l=0.2, 0.25, 0.3, 0.35 and 0.4) were studied and the basic geometric parameters for them are $l = 20\text{mm}$ and $\rho^*/\rho_s = 0.1$. Representative blocks for the honeycombs with three different joint geometries, which used as FE models, are illustrated in Fig.6. Three different levels of mesh sizes (1mm, 0.5mm and 0.25mm) were implemented in these honeycombs to conduct mesh sensitivity analyses. For the honeycombs with $r/l = 0.4$, the normalized moduli obtained from 1 mm mesh size are quite close to those obtained from the other two lower mesh sizes, as shown in Fig.7. It is to be expected that 1mm mesh size is suitable for all of the honeycombs.

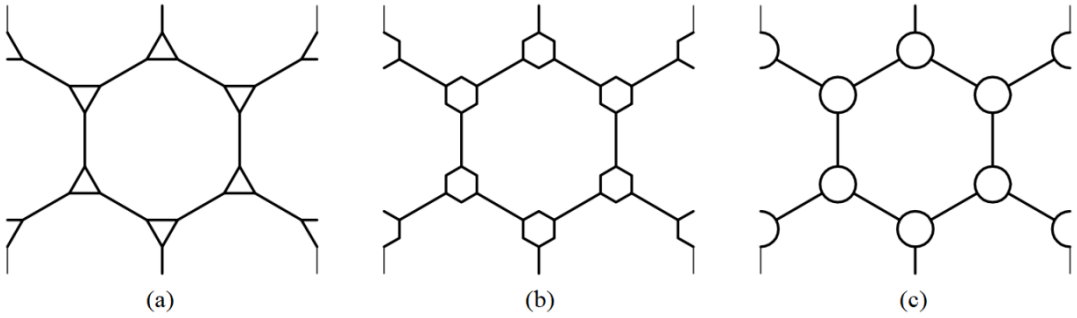

Fig.6. Representative blocks of the honeycombs used for FE models: (a) triangular joint honeycomb, (b) hexagonal joint honeycomb, (c) circular joint honeycomb. (Color online only)

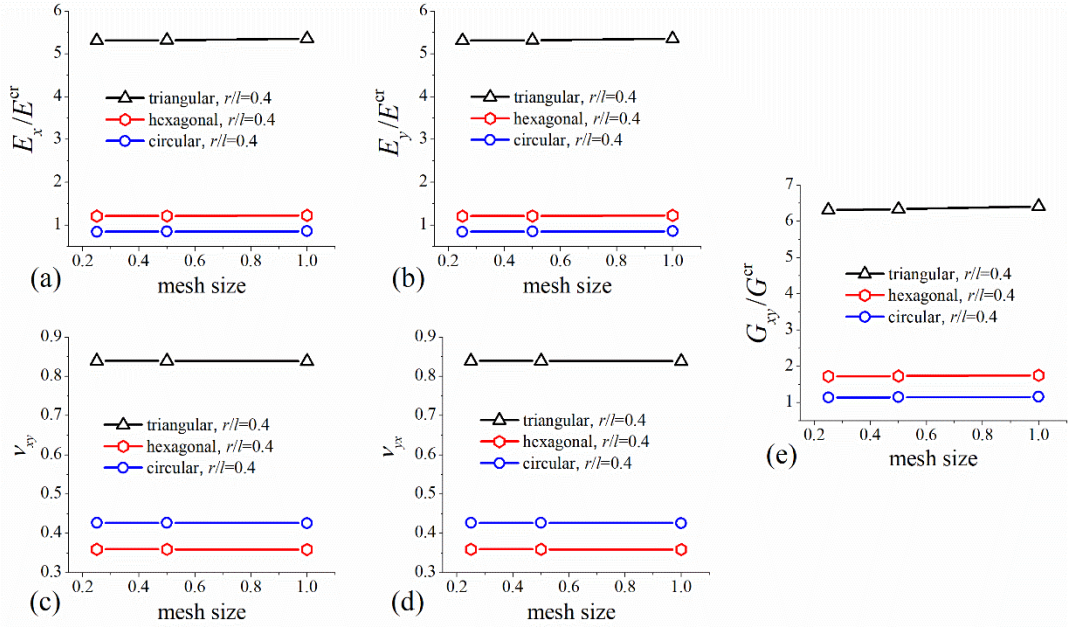

Fig.7. Mesh sensitivity analyses on the in-plane equivalent elastic moduli of the triangular joint, hexagonal joint and circular joint honeycombs while $\rho^*/\rho_s = 0.1$, $l = 20\text{mm}$ and $r = 8\text{mm}$ (i.e., r/l=0.4). (Color online only)

The variations of the equivalent Young's moduli and Poisson's ratios of the three different joint honeycombs with r/l are shown in Figs.8 and 9, respectively. The equivalent Young's moduli of these honeycombs are normalized by the equivalent Young's modulus of the convention regular hexagonal honeycomb (E^{cr}) with the same relative density. Analytical expressions for the equivalent Young's modulus of the convention regular hexagonal one, which was given by Gibson and Ashby (1997), are attached in Appendix C. From Figs.8 and 9, a quite good agreement between the present theoretical models and the FE simulations is obtained. For the hexagonal joint honeycomb, the present theoretical model is more accurate than the model given by Ajdari et al. (2012). This is because Ajdari et al. (2012) only considered the bending mechanism while the present theoretical model fully considered the axial and shear deformations of the walls in addition to bending. As the present theoretical models are able to describe the mechanical properties of the honeycombs accurately, the following discussion is only conducted based on these models. It can be also found from Figs.8 and 9 that the moduli in the x direction are very close to that in the y direction for all types of the honeycombs, i.e. $E_x = E_y$ and $\nu_{xy} = \nu_{yx}$, which reveals a macroscopic isotropic characteristic of these honeycombs. This phenomenon is consistent with the conclusion reported in the literature that plane lattices with threefold symmetry will exhibit macroscopically isotropic in-plane elastic behavior (Christensen, 1987).

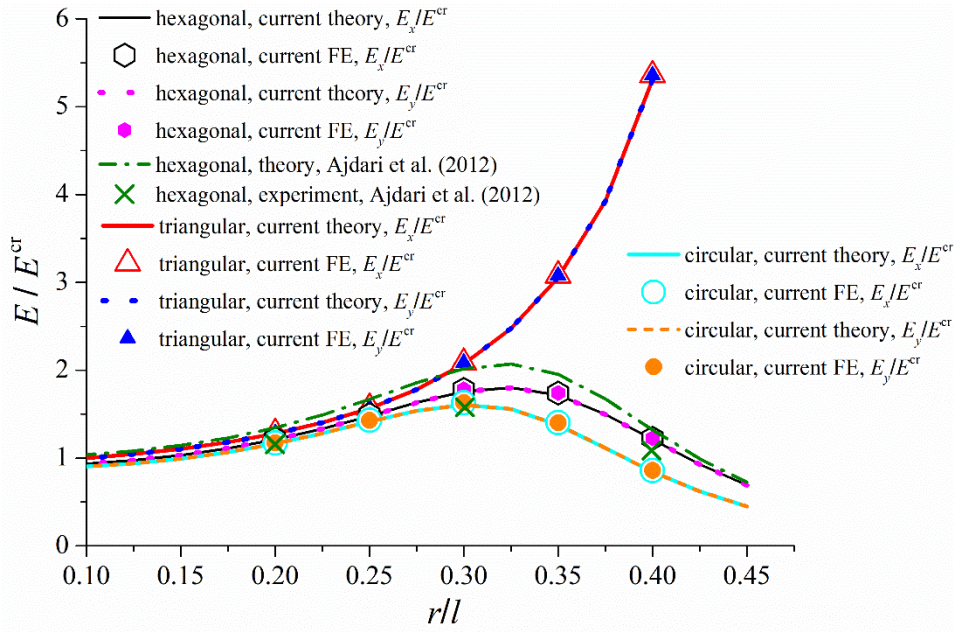

Fig.8. Normalized Young's modulus of the regular hexagonal honeycomb with three different joint geometries while $\rho^*/\rho_s = 0.1$ and $l = 20\text{mm}$: a comparison between the present theory, finite element simulations and the results from the literature (Ajdari et al., 2012). (Color online only)

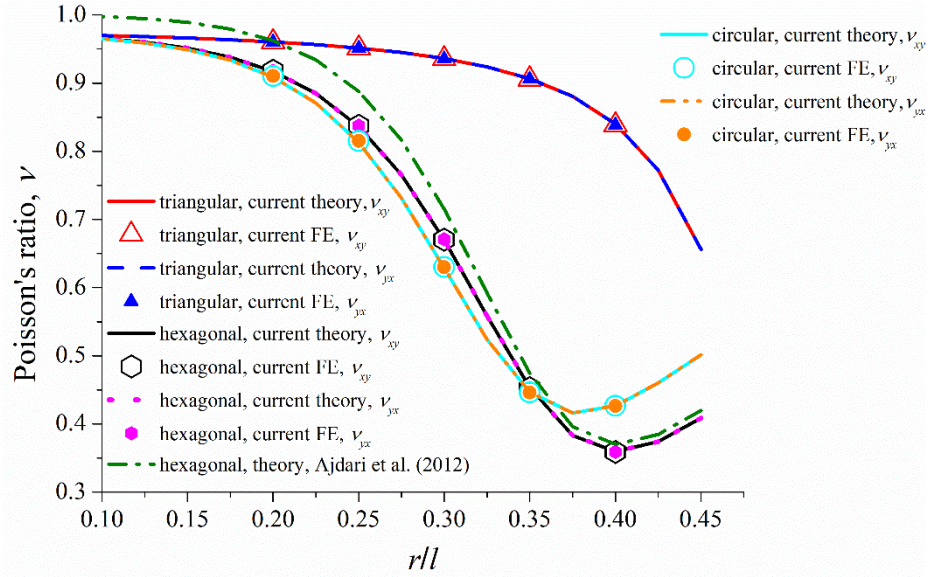

Fig.9. Poisson's ratio of the regular hexagonal honeycomb with three different joint geometries while $\rho^*/\rho_s = 0.1$ and $l = 20\text{mm}$: a comparison between the present theory, finite element simulations and the results from the literature (Ajdari et al., 2012). (Color online only)

In Fig.8, the normalized Young's moduli of both the hexagonal joint and circular joint honeycombs first increase and then decrease with r/l, while that of the triangular joint monotonously increases with r/l. The normalized moduli of these honeycombs are close to 1 when r/l tends to 0.1, indicating that the Young's moduli of these honeycombs tend to that of the conventional regular one at low level of r. The largest value of the normalized modulus ($E/E^{cr} = 1.61$) of the circular joint honeycomb appears at $r/l = 0.3$ while that of the hexagonal joint honeycomb ($E/E^{cr} = 1.80$) appears at $r/l = 0.325$. This means that the Young's modulus of the circular joint and hexagonal joint honeycombs are enhanced by 61% and 80%, respectively, compared to the conventional regular one, while for the triangular joint honeycomb, its Young's modulus is improved by 107% at $r/l = 0.3$ and even 431% at $r/l = 0.4$.

It is shown that the Young's modulus of the circular joint honeycomb is the lowest while that of the triangular joint honeycomb is the highest among the three joint honeycombs. Obviously, the stiffness of the circular joint honeycomb is slightly lower than that of the hexagonal joint one for all r/l. For the triangular joint

honeycomb, its stiffness is not very different from that of the other two honeycombs when r/l varies from 0.1 to 0.25. However, after $r/l > 0.25$, the stiffness gap between the triangular honeycomb and the other two honeycombs is getting bigger. This phenomenon can be explained by the fact that the joint itself has little effect on the stiffness of these honeycombs when r/l is small and the main contributor is the wall connecting each two joints. Taking Fig.2(b) as an example, when r/l is small, the deformations of the walls BC and DE are the major factor in response to an external stress while the joint ABD will have little effect. However, when r/l is getting big, the effect of the joint ABD will become significant. It is important to note that axial deformation is the dominated mechanism within a triangular joint while the circular and hexagonal joints are both bending controlled. Consequently, the stiffness of the triangular joint honeycomb is much higher than that of the circular and hexagonal joint ones when r/l becomes big. From this point of view, the triangular joint honeycomb is more successful in micro-structural layout compared with the other two honeycombs.

As shown in Fig.9, the Poisson's ratio of the triangular joint honeycomb is higher than that of the other two honeycombs. At low level of r/l, e.g. $r/l = 0.1$, the Poisson's ratios of these honeycombs are very close to 1. With r/l increasing, ν of the triangular joint honeycomb monotonously decreases while that of the circular and hexagonal joint honeycombs first decrease to a valley and then increase. For the circular joint honeycomb, the minimum value of ν ($\nu = 0.416$) is observed at $r/l = 0.375$ while the minimum value ($\nu = 0.360$) for the hexagonal joint honeycomb appears at $r/l = 0.4$.

3.2. Shear moduli

For isotropic cellular solids, their in-plane equivalent Yong's modulus (E), Poisson's ratio (ν) and shear modulus (G) approximately obeys the following relation Gibson and Ashby (1997):

$$G = \frac{E}{2(1+\nu)}. \tag{18}$$

As shown from both the theoretical and FE results in section 3.1, the honeycombs in this study are all macroscopically isotropic. As a result, the equivalent shear moduli of these honeycombs can be readily calculated using Eq.(18). For comparison, the FE method with periodic boundary conditions was also used to predict the in-plane shear

modulus of the honeycombs with three different joint geometries. Detailed boundary conditions for in-plane shear loading are listed as Eq.(14). From Fig.7, 1mm mesh size was used for these simulations.

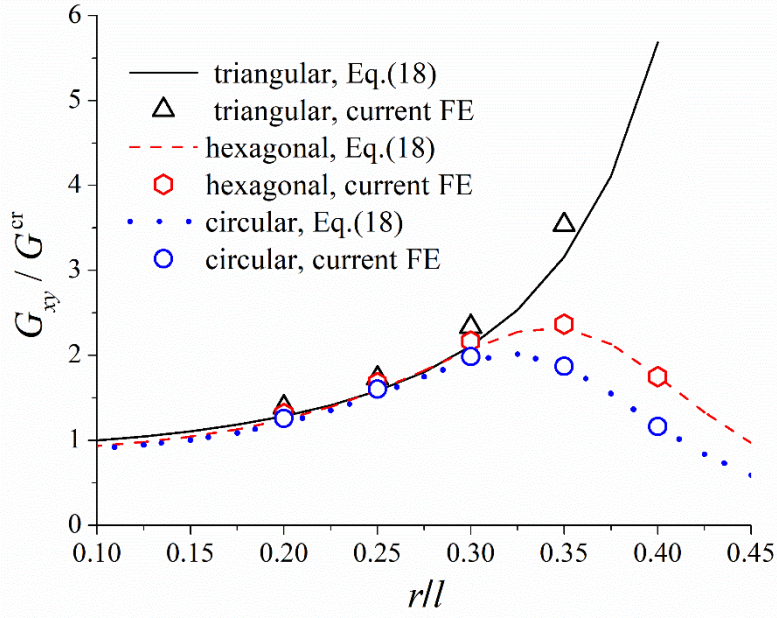

Fig.10. FE and theoretical predictions of the in-plane shear modulus of the honeycombs versus r/l while $\rho^*/\rho_s = 0.1$ and $l = 20\text{mm}$. (Color online only)

Fig.10 shows the FE and theoretical predictions of in-plane shear moduli versus r/l while $\rho^*/\rho_s = 0.1$ and $l = 20\text{mm}$. It is found in that the theoretical predictions from Eq.(18) are close to the FE simulations. The shear moduli of the three joint honeycombs are normalized by the shear stiffness of the conventional regular hexagonal honeycomb which is shown in Appendix C. The normalized values are quite close to 1 when r/l is small, i.e., $r/l = 0.1$. This means that the shear moduli of these honeycombs are close to that of the conventional regular one at low r/l. It is noted that the normalized modulus of the triangular joint honeycomb monotonously increases with r/l while those of both the hexagonal joint and circular joint honeycombs first increase to a peak and then decrease with r/l. According to the theoretical predictions, the peak value for the hexagonal joint honeycomb appears at $r/l = 0.35$ and equals 2.33. This means that the shear modulus of the hexagonal joint honeycomb is enhanced by 133% when $r/l = 0.35$, compared to the conventional regular one. Similarly, the shear modulus of the circular joint honeycomb is improved

by 101% when r/l is 0.325. For the triangular joint honeycomb, improvement of its shear modulus can reach 469%.

3.3. Effect of ρ^*/ρ_s

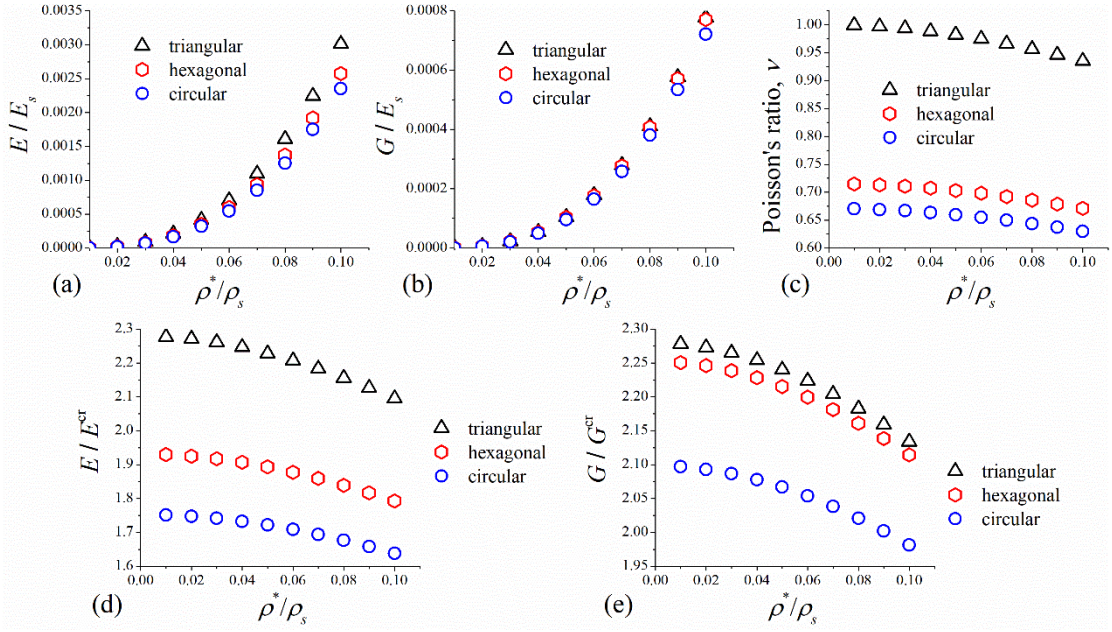

Fig.11. Variations of the equivalent moduli of the three honeycombs with relative density (ρ^*/ρ_s) while $r = 6\text{mm}$, $l = 20\text{mm}$: (a) Young's moduli normalized by the Young's modulus of the basic material, E_s; (b) shear moduli normalized by the Young's modulus of the basic material, E_s; (c) Poisson's ratios; (d) Young's moduli normalized by the Young's modulus of the conventional regular hexagonal honeycomb, E^{cr}; (e) shear moduli normalized by the shear modulus of the conventional regular hexagonal honeycomb, G^{cr}.(Color online only)

We have discussed the effect of r/l on the in-plane Young's moduli and shear moduli previously while $\rho^*/\rho_s = 0.1$. In this section, we focus on the influence of the relative density, ρ^*/ρ_s, on the equivalent moduli under a fixed r/l. In this investigation, the basic geometric parameters $l = 20\text{mm}$ and $r = 6\text{mm}$ were adopted. Increasing the relative density ρ^*/ρ_s, the Young's moduli and shear moduli of the three honeycombs, which are normalized by the Young's modulus of the basic material (E_s), monotonously increase, as shown in Fig.11 (a) and (b). On the contrary, the Poisson's ratios monotonously decreases with ρ^*/ρ_s (see Fig.11(c)). Fig.11(d)

and (e) respectively show the variations of the Young's moduli and shear moduli of the honeycombs, which are normalized by the moduli of the conventional regular honeycomb, with ρ^*/ρ_s. One can find that both E/E_{cr} and G/G_{cr} monotonously decrease with ρ^*/ρ_s. On can find from Fig.11 (a) to (e) that, the equivalent elastic moduli of the triangular joint honeycomb (i.e., normalized Young's modulus, normalized shear modulus and Poisson's ratio) are higher than those of the other two types of honeycombs under the same relative density, meanwhile, those moduli of the circular joint honeycomb are the lowest.

4. Concluding remarks

By using the theoretical and FE methods, three types of homologous hexagonal honeycombs, which are derived by replacing each three-wall vertex of a conventional regular hexagonal honeycomb with a small circle, a hexagon and a triangle, were investigated in this paper. We discussed the effects of ρ^*/ρ_s and r/l on the elastic moduli of these honeycombs. A comparison among these honeycombs was also conducted. Some conclusions are drawn as follows:

1) The normalized Young's modulus (E/E^{cr}) and shear modulus (G/G^{cr}) of the hexagonal and circular joint honeycombs vary with r/l in a unimodal way while those of the triangular joint honeycomb monotonously increase with r/l. Compared to the conventional regular hexagonal honeycomb, the Young's modulus of the circular joint, hexagonal joint, and triangular joint honeycombs are enhanced by 61%, 80% and 431%, respectively; while the shear modulus are improved by 101%, 133% and 469%, respectively. As a result, the triangular joint honeycomb exhibits higher stiffness than the other two honeycombs.

2) At low level of r/l, the Poisson's ratio values of these honeycombs are quite close to 1. With r/l increasing, the Poisson's ratio of the triangular joint honeycomb monotonously decreases, while that of the other two honeycombs decreases to a valley and then increases. The minimum values of the Poisson's ratio are 0.416 and 0.360 respectively for the circular and hexagonal joint honeycombs.

3) The normalized Young's modulus (E/E^{cr}), shear modulus (G/G^{cr}) and Poisson's ratio of these honeycombs monotonously decreases with ρ^*/ρ_s,

indicating that, compared to the conventional regular hexagonal honeycomb, the advantage in stiffness of these honeycombs is more prominent under the case of low ρ^* / ρ_s.

This work is focused only on the elastic properties of regular hexagonal honeycomb with three different joints, and the dynamic responses of these structures will be presented in our next paper.

Acknowledgements

The authors would like to thank the funding support from the Research Grants Council of Hong Kong Special Administrative Region Government (grant number: 15209616) and The Hong Kong Polytechnic University (internal project reference: YBUZ).

Conflict of interest statement

The authors declare that they have no conflict of interest.

Appendix A. Theoretical model for the hexagonal joint honeycomb

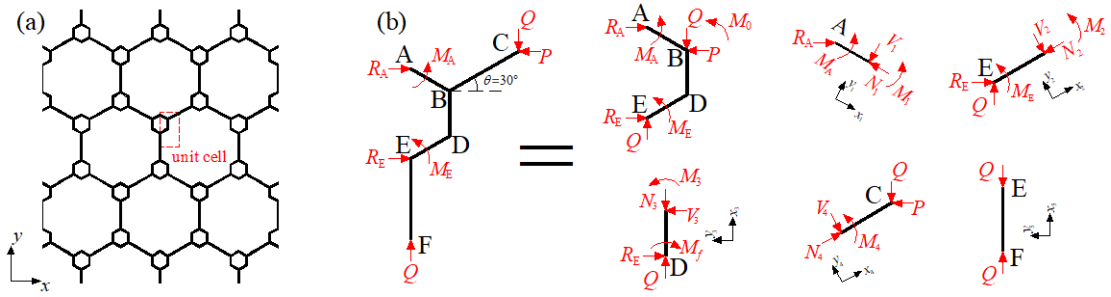

Fig.A.1. (a) Unit cell for the hexagonal joint honeycomb and (b) force analysis in a unit cell: unit cell under a x- directional uniaxial load P or a y- directional uniaxial load Q. x_i-y_i denotes the local coordinate system for each wall. (Color online only)

From Fig.A.1, the total strain energy stored in the unit cell ABCDEF, U_2, is composed of five components, i.e.,

$$U_2 = U_{\mathrm{AB}} + U_{\mathrm{ED}} + U_{\mathrm{BD}} + U_{\mathrm{BC}} + U_{\mathrm{EF}}, \tag{A1}$$

where U_{AB}, U_{ED}, U_{BD}, U_{BC} and U_{EF} are the strain energies stored in the walls AB, ED, BD, BC and EF, respectively. The axial force, shear force and bending moment acting at each wall can be obtained from Fig.A.1(b). They are listed below:

AB: $N_1(x_1) = R_{\mathrm{A}}\cos(\pi/6)$, $V_1(x_1) = R_{\mathrm{A}}\sin(\pi/6)$, $M_1(x_1) = -M_{\mathrm{A}} + R_{\mathrm{A}}\sin(\pi/6)x_1$;

ED: $N_2(x_2) = R_{\mathrm{E}}\cos(\pi/6) + Q\sin(\pi/6)$, $V_2(x_2) = Q\cos(\pi/6) - R_{\mathrm{E}}\sin(\pi/6)$,

$M_2(x_2) = -M_{\mathrm{E}} + \left[Q\cos(\pi/6) - R_{\mathrm{E}}\sin(\pi/6)\right]x_2$;

BD: $N_3(x_3) = Q$, $V_3(x_3) = R_{\mathrm{E}}$, $M_3(x_3) = M_f - R_{\mathrm{E}}(x_3)$

(where $M_f = M_2(x_2)\big|_{x_2=r} = -M_{\mathrm{E}} + \left[Q\cos(\pi/6) - R_{\mathrm{E}}\sin(\pi/6)\right]r$);

BC: $N_4(x_4) = P\cos\theta + Q\sin\theta$, $V_4(x_4) = P\sin\theta - Q\cos\theta$,

$M_4(x_4) = -(P\sin\theta - Q\cos\theta)(l/2 - r - x_4)$;

EF: $N_5(x_5) = Q$, $V_5(x_5) = 0$, $M_5(x_5) = 0$.

Then the strain energy stored in each wall is further calculated as:

$$U_{\mathrm{AB}}=\frac{R_{\mathrm{A}}{}^{2}\cos^{2}\left(\pi/6\right)r}{2E_{s}A}+\frac{kR_{\mathrm{A}}{}^{2}\sin^{2}\left(\pi/6\right)r}{2G_{s}A}+\frac{M_{\mathrm{A}}{}^{2}r}{2E_{s}I}+\frac{R_{\mathrm{A}}{}^{2}\sin^{2}\left(\pi/6\right)r^{3}}{6E_{s}I}-\frac{M_{\mathrm{A}}R_{\mathrm{A}}\sin\left(\pi/6\right)r^{2}}{2E_{s}I};$$

$$U_{\mathrm{ED}}=\frac{\left[R_{\mathrm{E}}\cos\left(\pi/6\right)+Q\sin\left(\pi/6\right)\right]^{2}r}{2E_{s}A}+\frac{k\left[Q\cos\left(\pi/6\right)-R_{\mathrm{E}}\sin\left(\pi/6\right)\right]^{2}r}{2G_{s}A}+\frac{M_{\mathrm{E}}{}^{2}r}{2E_{s}I}+$$

$$\frac{\left[Q\cos\left(\pi/6\right)-R_{\mathrm{E}}\sin\left(\pi/6\right)\right]^{2}r^{3}}{6E_{s}I}-\frac{M_{\mathrm{E}}\left[Q\cos\left(\pi/6\right)-R_{\mathrm{E}}\sin\left(\pi/6\right)\right]r^{2}}{2E_{s}I};$$

$$U_{\mathrm{BD}}=\frac{Q^{2}r}{2E_{s}A}+\frac{kR_{\mathrm{E}}{}^{2}r}{2G_{s}A}+\frac{\left\{\left[Q\cos\left(\pi/6\right)-R_{\mathrm{E}}\sin\left(\pi/6\right)\right]r-M_{\mathrm{E}}\right\}^{2}r}{2E_{s}I}+\frac{R_{\mathrm{E}}{}^{2}r^{3}}{6E_{s}I}-$$

$$\frac{\left\{-M_{\mathrm{E}}+\left[Q\cos\left(\pi/6\right)-R_{\mathrm{E}}\sin\left(\pi/6\right)\right]r\right\}R_{\mathrm{E}}r^{2}}{2E_{s}I};$$

$$U_{\mathrm{BC}}=\frac{\left(P\cos\theta+Q\sin\theta\right)^{2}\left(l/2-r\right)}{2E_{s}A}+\frac{k\left(P\sin\theta-Q\cos\theta\right)^{2}\left(l/2-r\right)}{2G_{s}A}+\frac{\left(P\sin\theta-Q\cos\theta\right)^{2}\left(l/2-r\right)^{3}}{6E_{s}I};$$

$$U_{\mathrm{EF}}=\frac{Q^{2}\left(l/2-r\right)}{E_{s}A}.$$

(A2)

where

$$M_{0}=\left(P\sin\theta-Q\cos\theta\right)\left(l/2-r\right),$$

$$M_{\mathrm{E}}=-M_{\mathrm{A}}-M_{0}+Qr\cos\left(\pi/6\right)+Pr\sin\left(\pi/6\right)-R_{\mathrm{E}}\left[r+2r\sin\left(\pi/6\right)\right],$$

$$R_{\mathrm{E}}=P-R_{\mathrm{A}}.$$

Considering the boundary conditions of the unit cell, i.e., $\partial U_{2}/\partial R_{\mathrm{A}}=0$ and $\partial U_{2}/\partial M_{\mathrm{A}}=0$, we have,

$$\begin{cases}\left(\dfrac{3r}{2E_{s}A}+\dfrac{3kr}{2G_{s}A}+\dfrac{17r^{3}}{4E_{s}I}\right)\cdot R_{\mathrm{A}}-\dfrac{3r^{2}}{E_{s}I}\cdot M_{\mathrm{A}}=\dfrac{\left(3P+\sqrt{3}Q\right)r}{4E_{s}A}+\dfrac{kr\left(5P-\sqrt{3}Q\right)}{4G_{s}A}+\dfrac{11M_{0}r^{2}}{4E_{s}I}+\dfrac{67Pr^{3}}{24E_{s}I}+\\ \dfrac{5Qr^{3}}{4\sqrt{3}E_{s}I}-\dfrac{7\sqrt{3}Qr^{3}}{8E_{s}I};\\ -\dfrac{3r^{2}}{E_{s}I}\cdot R_{\mathrm{A}}+\dfrac{3r}{E_{s}I}\cdot M_{\mathrm{A}}=\dfrac{\sqrt{3}Qr^{2}}{4E_{s}I}-\dfrac{2M_{0}r}{E_{s}I}-\dfrac{7Pr^{2}}{4E_{s}I}.\end{cases}$$

(A3)

From the two relations in Eq.(A3), we can express R_{A} and M_{A} as a known function of the forces P and Q. Hence, the total strain energy U_{2} can also be

written as a known function of P and Q. Finally, the equivalent Young's modulus and Poisson's ratio for the hexagonal joint honeycomb can be calculated by using the similar derivations as shown in section 3.1.

Appendix B. Theoretical model for the circular joint honeycomb

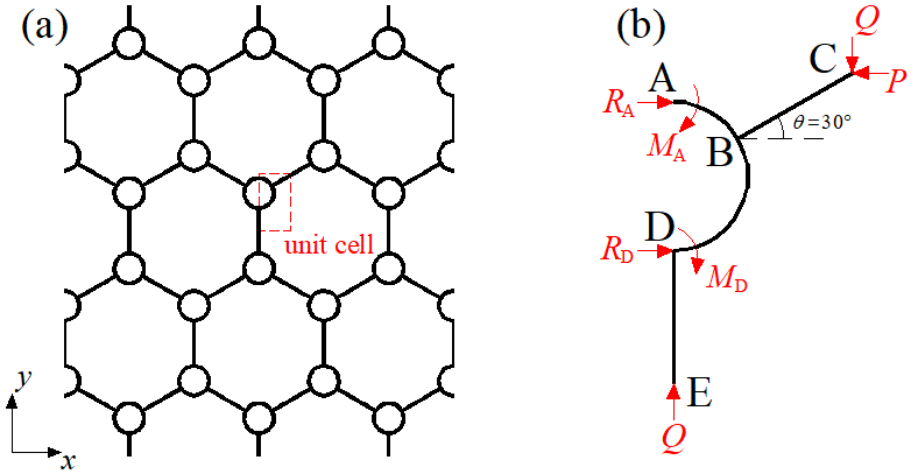

Fig.B.1. (a) Unit cell of the circular joint honeycomb and (b) force analysis in a unit cell: unit cell under a *x*- directional uniaxial load P or a *y*- directional uniaxial load Q. (Color online only)

As shown by Chen et al. (2014), the total strain energy, U_3, of the unit cell of the circular joint honeycomb is composed of four parts, the energies stored in the semicircle AB, semicircle BD, walls BC and DE. In this paper, we will not repeat the force analyses of each semicircle or wall as they were fully presented by Chen et al. (2014). By using those force analyses, we recalculate the strain energy for each part as:

$$U_{\mathrm{AB}}=\frac{\left(3\sqrt{3}+4\pi\right)r}{48E_sA}R_{\mathrm{A}}{}^2-\frac{k\left(3\sqrt{3}-4\pi\right)r}{48G_sA}R_{\mathrm{A}}{}^2+\frac{r\left[8M_{\mathrm{A}}{}^2\pi+8M_{\mathrm{A}}R_{\mathrm{A}}\left(3\sqrt{3}-2\pi\right)r+3R_{\mathrm{A}}{}^2\left(-7\sqrt{3}+4\pi\right)r^2\right]}{48E_sI};$$

$$U_{\mathrm{BD}}=\frac{r\left\{8\pi\left[Q^2+\left(P-R_{\mathrm{A}}\right)^2\right]-3\left[\sqrt{3}P^2-\sqrt{3}Q^2+6QR_{\mathrm{A}}+\sqrt{3}R_{\mathrm{A}}{}^2-2P\left(3Q+\sqrt{3}R_{\mathrm{A}}\right)\right]\right\}}{48E_sA}+$$

$$\frac{kr\left\{8\pi\left[Q^2+\left(P-R_{\mathrm{A}}\right)^2\right]+3\left[\sqrt{3}P^2-\sqrt{3}Q^2+6QR_{\mathrm{A}}+\sqrt{3}R_{\mathrm{A}}{}^2-2P\left(3Q+\sqrt{3}R_{\mathrm{A}}\right)\right]\right\}}{48G_sA}+$$

$$\frac{r\left\{16\left(M_0+M_{\mathrm{A}}\right)^2\pi+8r\left(M_0+M_{\mathrm{A}}\right)\left[2\pi\left(P-\sqrt{3}Q-2R_{\mathrm{A}}\right)+3\sqrt{3}P+9Q-3\sqrt{3}R_{\mathrm{A}}\right]\right\}}{48E_sI}+$$

$$\frac{\pi r^3\left[3P^2+5Q^2-2\sqrt{3}Q\left(P-2R_{\mathrm{A}}\right)-8PR_{\mathrm{A}}+6R_{\mathrm{A}}{}^2\right]}{12E_sI}+$$

$$\frac{r^3\left(3\sqrt{3}P^2+6PQ-11\sqrt{3}Q^2-10\sqrt{3}PR_{\mathrm{A}}-18QR_{\mathrm{A}}+7\sqrt{3}R_{\mathrm{A}}{}^2\right)}{16E_sI};$$

$$U_{\mathrm{BC}}=\frac{\left(P\cos\theta+Q\sin\theta\right)^2\left(l/2-r\right)}{2E_sA}+\frac{k\left(P\sin\theta-Q\cos\theta\right)^2\left(l/2-r\right)}{2G_sA}+\frac{\left(P\sin\theta-Q\cos\theta\right)^2\left(l/2-r\right)^3}{6E_sI};$$

$$U_{\mathrm{DE}}=\frac{Q^2\left(l/2-r\right)}{E_sA}.$$

(B1)

where $M_0=\left(P\sin\theta-Q\cos\theta\right)\left(l/2-r\right)$, $M_{\mathrm{D}}=-M_{\mathrm{A}}-M_0+\sqrt{3}Qr/2+Pr/2-2R_{\mathrm{D}}r$

and $R_{\mathrm{D}}=P-R_{\mathrm{A}}$.

Using the boundary conditions: $\partial U_3/\partial R_{\mathrm{A}}=0$ and $\partial U_3/\partial M_{\mathrm{A}}=0$, we have,

$$\begin{cases}\left(\dfrac{\pi r}{2E_sA}+\dfrac{k\pi r}{2G_sA}+\dfrac{3\pi r^3}{2E_sI}\right)\cdot R_{\mathrm{A}}-\dfrac{\pi r^2}{E_sI}\cdot M_{\mathrm{A}}=\dfrac{\left(5\sqrt{3}P+9Q\right)r^3}{8E_sI}-\dfrac{\left(\sqrt{3}Q-2P\right)\pi r^3}{3E_sI}-\dfrac{M_0\left(-3\sqrt{3}-4\pi\right)r^2}{6E_sI}-\\ \dfrac{3\sqrt{3}Pr-8P\pi r-9Qr}{24E_sA}-\dfrac{k\left(-3\sqrt{3}Pr-8P\pi r+9Qr\right)}{24G_sA};\\ -\dfrac{\pi r^2}{E_sI}\cdot R_{\mathrm{A}}+\dfrac{\pi r}{E_sI}\cdot M_{\mathrm{A}}=\dfrac{\pi r^2\left(\sqrt{3}Q-P\right)}{3E_sI}-\dfrac{2M_0\pi r}{3E_sI}-\dfrac{\left(\sqrt{3}P+3Q\right)r^2}{2E_sI}.\end{cases}$$

(B2)

Similarly, the total strain energy U_3 ($U_3=U_{\mathrm{AB}}+U_{\mathrm{BD}}+U_{\mathrm{BC}}+U_{\mathrm{DE}}$) can be expressed

as a known function of P and Q, and thus the in-plane equivalent modulus can be finally obtained.

Appendix C. Elastic moduli of the conventional regular hexagonal honeycomb

With fully considering the axial and shear deformation as well as bending of the cell walls, the in-plane equivalent Young's modulus, Poisson's ratio and shear modulus of the conventional regular hexagonal honeycomb were given by Gibson and Ashby (1997):

$$\begin{aligned}
\frac{E^{\mathrm{cr}}}{E_s} &= \frac{4}{\sqrt{3}}\left(\frac{t}{l}\right)^3 \frac{1}{1+\left(5.4+1.5\nu_s\right)\left(t/l\right)^2}; \\
\nu^{\mathrm{cr}} &= \frac{1+\left(1.4+1.5\nu_s\right)\left(t/l\right)^2}{1+\left(5.4+1.5\nu_s\right)\left(t/l\right)^2}; \\
\frac{G^{\mathrm{cr}}}{E_s} &= \frac{1}{\sqrt{3}}\left(\frac{t}{l}\right)^3 \frac{1}{1+\left(3.30+1.75\nu_s\right)\left(t/l\right)^2}.
\end{aligned} \tag{C1}$$

References

Ajdari, A., Jahromi, B. H., Papadopoulos, J., Nayeb-Hashemi, H., Vaziri, A., 2012. Hierarchical honeycombs with tailorable properties. International Journal of Solids and Structures 49,1413-1419.

Ai, L., Gao, X. L., 2018. Three-dimensional metamaterials with a negative Poisson's ratio and a non-positive coefficient of thermal expansion. International Journal of Mechanical Sciences 135, 101-113.

Balawi, S., Abot, J. L., 2008. The effect of honeycomb relative density on its effective in-plane elastic moduli: an experimental study. Compos. Struct. 84, 293-299.

Christensen, R. M., 1987. Sufficient symmetry conditions for isotropy of the elastic moduli tensor. J. Appl. Mech. 54,772-777.

Chuang, C. H., Huang, J. S., 2002a. Effects of solid distribution on the elastic buckling of honeycombs. International Journal of Mechanical Sciences 44,1429-1443.

Chuang, C. H., Huang, J. S., 2002b. Elastic moduli and plastic collapse strength of

hexagonal honeycombs with plateau borders. International Journal of Mechanical Sciences 44,1827-1844.

Cricrì, G., Perrella, M., Calì, C., 2013. Honeycomb failure processes under in-plane loading. Composites: Part B 45,1079-1090.

Catapano, A., Montemurro, M., 2014. A multi-scale approach for the optimum design of sandwich plates with honeycomb core. Part I: homogenisation of core properties. Compos. Struct. 118, 664-676.

Chen, Q., Pugno, N., Zhao, K., Li, Z., 2014. Mechanical properties of a hollow-cylindrical-joint honeycomb. Composite Structures 109, 68-74.

El-Sayed, F. K. A., Jones, R., Burgess, I. W., 1979. A theoretical approach to the deformation of honeycomb based composite materials. Composites 10(4),209-214.

Gibson, L.J., 1981. The elastic and plastic behaviour of cellular materials. University of Cambridge.

Gibson, L.J., Ashby, M.F., Schajer, G.S., Robertson, C.I., 1982. The mechanics of two-dimensional cellular materials. Proc. Roy. Soc. Lond. A 382, 25-42.

Gibson, L.J., Ashby, M.F., 1988. Cellular Solids: Structure and Properties, first edit. ed. Pergamon Press, Oxford.

Gibson, L. J., Ashby, M. F., 1997. Cellular Solids: Structure and Properties, second edit. Cambridge University Press, New York.

Gonella, S., Ruzzene, M., 2008. Homogenization and equivalent in-plane properties of two-dimensional periodic lattices. International Journal of Solids & Structures, 45(10), 2897-2915.

Hu, L. L., Yu, T. X., 2010. Dynamic crushing strength of hexagonal honeycombs. International journal of impact engineering, 37(5), 467-474.

Hu, L. L., Yu, T. X., 2013. Mechanical behavior of hexagonal honeycombs under low-velocity impact-theory and simulations. International Journal of Solids and Structures 50(20-21),3152-3165.

Karakoi, A., Freund, J., 2012. Experimental studies on mechanical properties of cellular structures using nomex® honeycomb cores. Composite Structures, 94(6), 2017-2024.

Lan, L. H., Fu, M. H., 2009. Nonlinear constitutive relations of cellular materials.

AIAA Journal 47(1), 264-270.

Masters, I. G., Evans, K. E., 1996. Models for the elastic deformation of honeycombs. Compos. Struct. 35, 403-422.

Malek, S., Gibson L., 2015. Effective elastic properties of periodic hexagonal honeycombs Mechanics of Materials 91, 226-240.

Papka, S., D., Kyriakides, S., 1994. In-plane compressive response and crushing of honeycomb. Journal of the Mechanics and Physics of Solids 42(10), 1499-1532.

Pozniak, A. A., Smardzewski, J., Wojciechowski, K. W., 2013. Computer simulations of auxetic foams in two dimensions. Smart Materials and Structures 22, 084009 (11pp).

Qiu, K., Wang, Z., Zhang, W., 2016. The effective elastic properties of flexible hexagonal honeycomb cores with consideration for geometric nonlinearity. Aerospace Science and Technology 58,258-266.

Ruan, D., Lu, G., Wang, B,. Yu, T. X., 2003. In-plane dynamic crushing of honeycombs-a finiteelement study. International Journal of Impact Engineering 28,161-182.

Reis, F. D., Ganghoffer, J. F., 2012. Equivalent mechanical properties of auxetic lattices from discrete homogenization. Computational Materials Science, 51(1), 314-321.

Shi, G., Tong, P., 1995. The derivation of equivalent constitutive equations of honeycomb structures by a two scale method. Computational Mechanics 15(5),395-407.

Sun, Y., Wang, B., Pugno, N., Wang, B., Ding, Q., 2015. In-plane stiffness of the anisotropic multifunctional hierarchical honeycombs. Composite Structures 131, 616-624.

Sorohan, S., Constantinescu, D. M., Sandu, M., Sandu, A., G., 2018. On the homogenization of hexagonal honeycombs under axial and shear loading. Part I: Analytical formulation for free skin effect. Mechanics of Materials 119,74-91.

Warren, W.E., Kraynik, A.M., 1987. Foam mechanics: the linear elastic response of two-dimensional spatially periodic cellular materials. Mech. Mater. 6, 27-37.

Xia, Z, Zhang, Y, Ellyin, F., 2003. A unified periodical boundary conditions for representative volume elements of composites and applications. International Journal

of Solids and Structures 40, 1907-1921.

Zhu, H. X., Mills, N. J., 2000. The in-plane non-linear compression of regular honeycombs. International Journal of Solids and Structures 37(13),1931-1949.

Zhang, Q., Yang, X., Li, P., Huang, G., Feng, S., Shen, C., Han, B., Zhang, X., Jin, F., Xu, F., Lu, T. J., 2015. Bioinspired engineering of honeycomb structure-Using nature to inspire human innovation. Progress in Materials Science 74, 332-400.

Zorzetto, L., Ruffoni, D., 2017. Re-entrant inclusions in cellular solids: From defects to reinforcements. Composite Structures 176,195-204.

Zhang, Y., Liua, T., Tizani, W., 2018. Experimental and numerical analysis of dynamic compressive response of Nomex honeycombs. Composites Part B 148,27-39.